Molecular Crystals and Liquid Crystals
Publication details, including instructions for authors and subscription information:
http://www.tandfonline.com/loi/gmcl16

Surface Tilt Distributions of Homogeneously Aligned Liquid Crystals

Richard W. Gurtler [a] & Jack W. Casey [a]
[a] Motorola, Inc., Phoenix, Arizona
Version of record first published: 28 Mar 2007.

To cite this article: Richard W. Gurtler & Jack W. Casey (1976): Surface Tilt Distributions of Homogeneously Aligned Liquid Crystals, Molecular Crystals and Liquid Crystals, 35:3-4, 275-306

To link to this article: http://dx.doi.org/10.1080/15421407608083678

Mol. Cryst. Liq. Cryst., 1976, Vol. 35, pp. 275–306

Printed in Holland

Surface Tilt Distributions of Homogeneously Aligned Liquid Crystals

RICHARD W. GURTLER and JACK W. CASEY

Motorola, Inc., Phoenix, Arizona

(*Received June 27, 1975; in final form March 19, 1976*)

The dielectric axes of surface molecules in a homogeneously aligned, nematic liquid crystal cell, have characteristic non-zero tilt orientations, $\delta\theta$, with respect to the bounding surface. An experimental technique is described which allows direct measurement of the average value of $\delta\theta$, $\langle\delta\theta\rangle$, as well as the distribution about $\langle\delta\theta\rangle$ over a finite surface area. A theoretical treatment of threshold behavior of a homogeneously aligned cell with a surface tilt boundary condition in the presence of a vertical electric field and a non-vertical magnetic field is presented which allows the quantitative interpretation of the experimental measurements. "Good" surfaces utilizing conventional rubbing techniques have sharp Gaussian distributions which are characteristic of the type of liquid crystal, surface composition and orientation technique. This procedure leads to a useful, quantitative technique to evaluate processing and orientation techniques as well as a means to study surface phenomena.

In order to capitalize fully on the unique and profound electro-optical properties of liquid crystals for display purposes, it is usually necessary to obtain thin layers of the liquid crystal in which the director axis is uniform or slowly changing in a prescribed manner. No abrupt changes in director axis are desired since such changes produce undesirable optical effects when uncontrolled. For example, for twisted nematic devices the well known[1] 90° helical twist orientation is desired where both the upper and lower surfaces of the layer are homogeneously aligned, but are rotated 90°, or nearly 90°, from each other. Due to aligning intermolecular forces, the layer assumes a helical twist.

Reducing the above to practice, however, has been somewhat of a problem for various reasons. Although it is easy to induce homogeneous alignment on pieces of glass by simply rubbing the glass in a uniform direction with almost anything in reach, it is another thing to produce almost perfectly homogeneous surfaces on multimaterial surfaces such as In–Sn–O strips on

glass, or metal–glass surfaces, and it is also difficult to find techniques which can perform well after subsequent high temperature processing or possibly chemical processing. Consequently a great deal of effort has been expended towards the obtaining of "hard" homogeneous surfaces capable of withstanding moderate to extreme temperatures (100°–500°C) together with being cost effective in a production environment.

In response to these needs, various techniques have been developed for achieving good quality homogeneous surfaces of various degrees of effectiveness. These techniques include the old "rubbing with lens paper," diamond polishing, utilization of chemical surfactants and high angle evaporation of metals and oxides onto the surface producing an inherent asymmetry at the surface for alignment purposes.

Testing of these surfaces is relatively straightforward: One fabricates test surfaces using some experimental technique and introduces a liquid crystal between two such plates in the proper manner and then evaluates the degree of extinction one may obtain between polarizers. This then is repeated for the same surfaces after stressing; e.g. high temperatures, cleaning procedures, etc. Although effective, this technqiue is quite subjective and is difficult to make quantitative. More quantitative and more sensitive methods are obviously needed. Before describing such an analytical method, a short discussion of twist and tilt domains is appropriate.

DOMAINS

Beyond the problem of obtaining high quality homogeneous surfaces it is necessary to obtain liquid crystal films which are "domain free." A domain is here meant to be a localized region where the director axis assumes a direction, either with or without a field applied, which differs from that of the intended or average direction of the surface as a whole. Such regions, as indicated previously, cause undesirable optical effects and detract from the appearance of the display. Two distinct types of domains are common.

TWIST DOMAINS

Twist domains are regions where the "handedness" of the helical twist abruptly changes across a domain wall, remaining constant, then abruptly changing back to the "preferred" handedness. Some characteristics of such domains are as follows: they have very sharp domain boundaries with or without an applied field and appear to require a discontinuity in director direction at some point of the boundary; the domain boundary is often

"pinned" by a dirt particle or other imperfection and if freed by mechanical agitation will often shrink and disappear; thermal cycling above and below the nematic point can create or destroy such domains; fabrication of displays with less than 90° twist energetically favors the region of smaller angle and serves to reduce the occurrence of twist domains; and finally, addition of cholesteric compounds which have an inherent handedness, can markedly reduce twist domains.

TILT DOMAINS

Of the two types of domains discussed here, the tilt domain is much simpler to analyze. This domain is most easily described in terms of a non-twisted cell but applies equally to a twisted cell. In Figure 1 a non-twisted, homogeneous cell is shown in an unactivated state together with the two possible states resulting from application of an electric field.

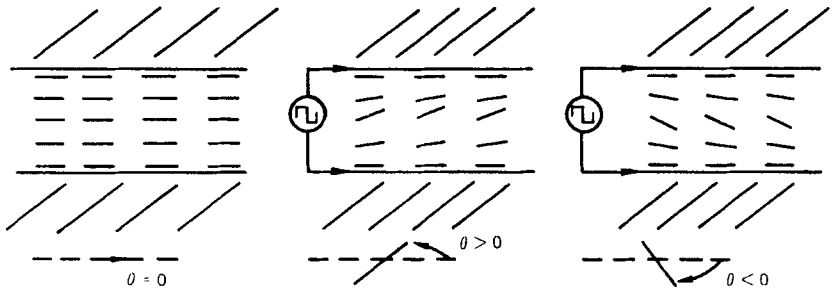

FIGURE 1 Bistable orientation of homogeneously aligned liquid crystals under the application of an electric field assuming no built-in preference towards positive or negative orientations.

If the electric field is strictly vertical and no preferential tilt to the molecules at the surface is assumed, then random thermal or current fluctuations will cause the director axis to choose between a positive or negative tilt. As this process is occurring over the entire surface, one could expect many regions of opposite tilt forming many "tilt" domains. The fact is, if the proper precautions are taken, a single preferred tilt direction results which can be predicted from the details of the polishing or aligning procedure. This means that some factor is present which is providing a preference for one tilt over the other.

TILT PREFERENCE MECHANISM

The most fundamental mechanism which provides a tilt preference is a small non-zero tilt of the molecules in the zero-field state which is characteristic of the molecular species, the polishing technique and the type of surface. Some experiments and theory describing this surface tilt, $\delta\theta$, will be presented below but first we should note that other effects may also cause a preference in certain cases which can override the influence of a tilt at the surface.

A non-vertical electric field is one means of providing a tilt preference and such is the case in the fringing field region of electrode edges; this is shown in Figure 2. It might be expected that such a region should exist for a distance roughly equal to the cell thickness and should be apparent only when the skewed field is inducing a non-preferred tilt direction—this is found to be true.

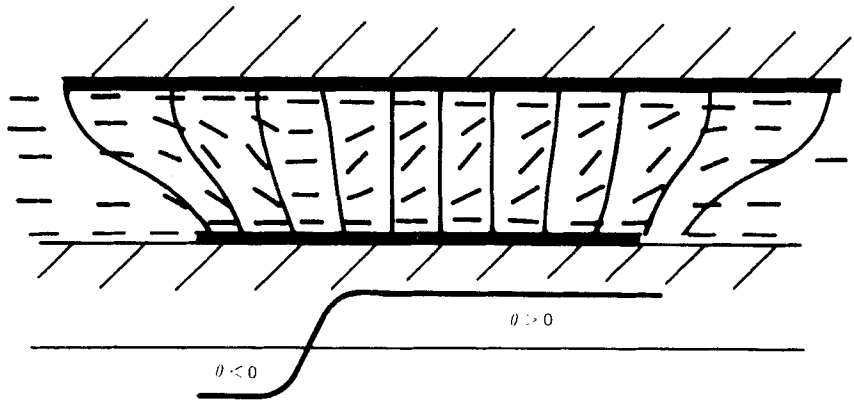

FIGURE 2 Fringing electrode fields and their influence on tilt orientation.

Other possible influences are from surface irregularities and current flow. The latter is especially easy to observe and is most pronounced when a cell has been allowed to relax quite fully, then is abruptly activated. As indicated in Figure 3, many small regions of non-preferred tilt are generated which usually soon vanish. If the cell is turned off and then back on with only a short interval to relax, the same regions tend to be created. If, however, the cell is allowed ample time to relax, entirely new regions will be formed—testifying to the random nature of the current induced distortions.

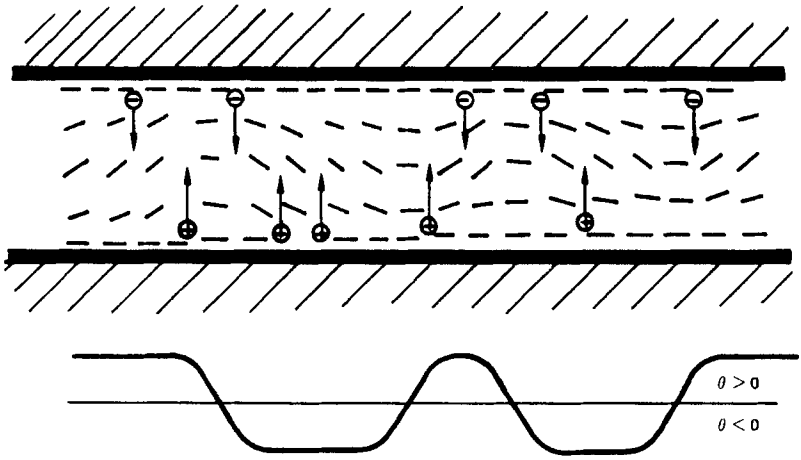

FIGURE 3 Orientation variations due to current induced turbulence.

SURFACE TILT PREFERENCE

Phenomenologically, what is supposed is that through a combination of polishing technique and surface and molecule composition, an effective non-zero tilt, $\delta\theta$, exists at the surface. If, as shown in Figure 4, the $\delta\theta$ angles on opposite surfaces match, then a constant $\theta = \delta\theta$ results throughout the film. If, on the other hand, they are opposite, then no effective tilt results. Experimentally these assumptions are verified and furthermore, the relationship of the polishing direction to $\delta\theta$, which is indicated in Figure 5, always seems to hold.

Exactly what is responsible for $\delta\theta$ is not the subject of this paper but let it be remembered that the physical, dielectric, optic and permeability axes are not necessarily the same and in fact are expected to be distinct. Consequently,

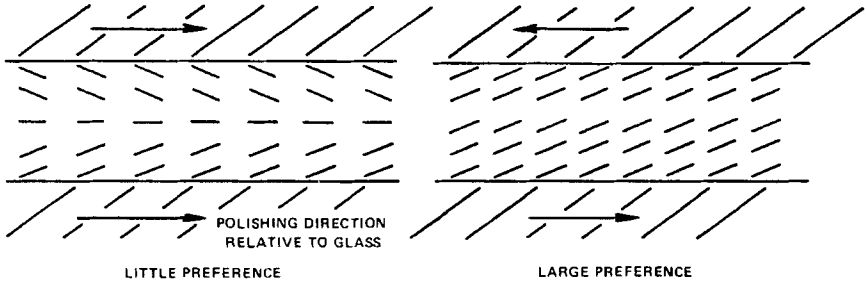

FIGURE 4 Influence of opposite surface tilt preference on the bulk orientation.

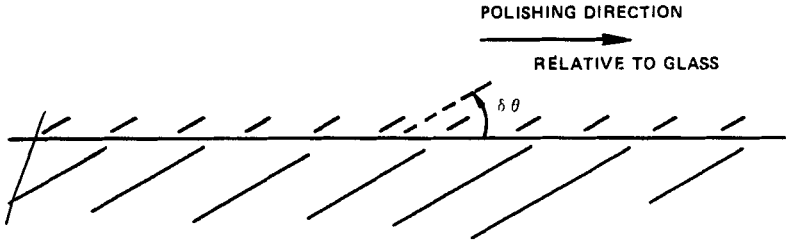

FIGURE 5 Surface tilt preference and polishing direction relationships.

if the bonding properties to the surface are such that the dielectric axis is not parallel to the surface then a preferred tilt direction results and if very uniform bonding is obtained then a very precise $\delta\theta$ can be expected.

EXPERIMENTAL

In order to study the effects of a finite surface tilt, $\delta\theta$, the experimental arrangement schematically illustrated in Figure 6 was utilized. This apparatus allowed the simultaneous application of a vertical electric field (relative to the liquid crystal film plane) due to conventional transparent electrodes within the sample cell, and a magnetic field which could be oriented at any angle relative to the sample normal by rotation of the sample holder about an axis perpendicular to the magnetic field.

Situated on both exterior surfaces of the sample cell were crossed polarizers which were oriented with respect to the polishing directions so as to give maximum transmission in an unactivated state. The polishing directions for the fabrication of the cells and sample mounting configurations were chosen so that the mid-film molecular orientation, the sample normal and the magnetic field were coplanar. The considerations of Figures 4 and 5 were utilized, although in this case for twisted cells, in order that the mid-film molecular orientation would acquire a maximum tilt preference. And finally, twist angles of about 80° were used to ensure the proper handedness of the twist. Figure 7 illustrates the relationships of the polishing directions to the sample cell. The indicated polishing directions yield a mid-film orientation along the sample axis and a tilt preference towards the sample normal.

The effects of the electric and magnetic fields on the molecular orientation were determined by LED-photodiode pairs oriented at 0° and $\pm 45°$ to the sample normal but lying in the plane containing the magnetic field and the sample normal.

In an unactivated state, the tilt preference is very small and would be difficult to measure directly. But on application of an electric field, the small

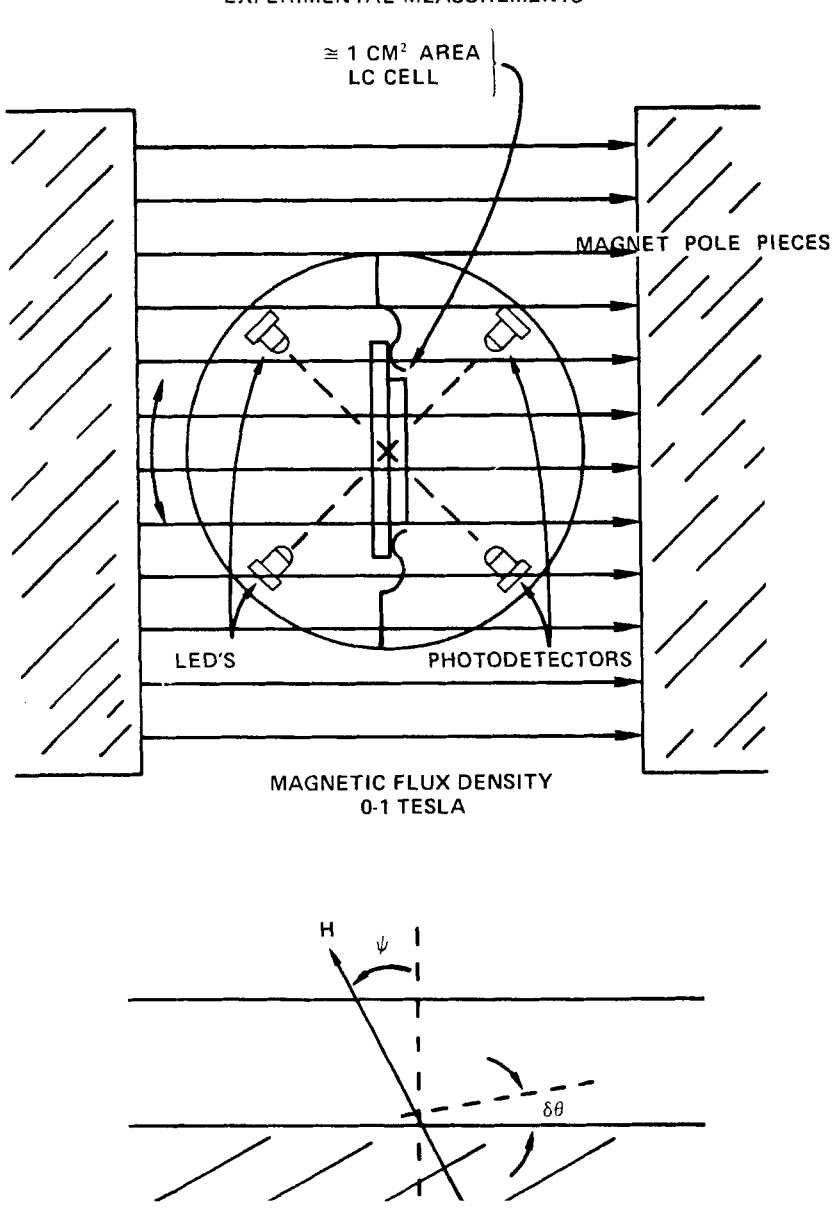

FIGURE 6 Experimental arrangement used to study surface tilt preferences.

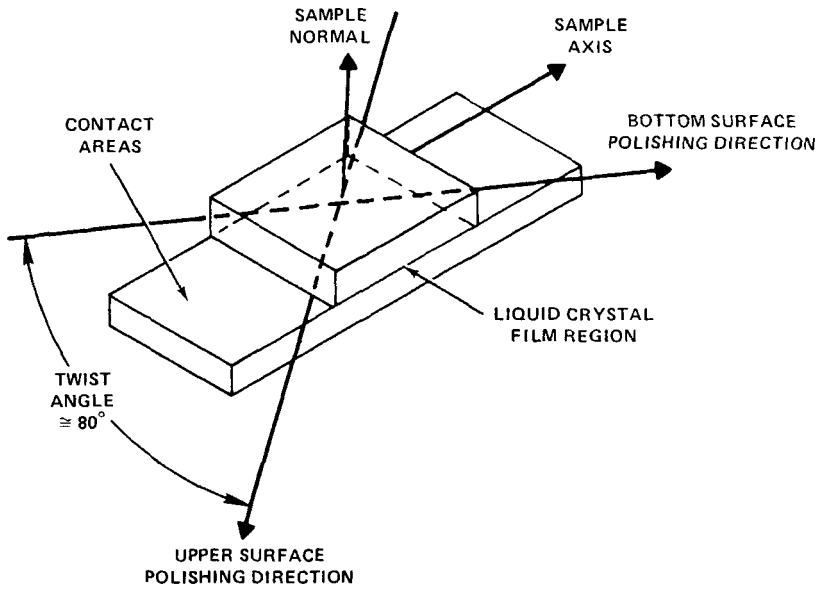

FIGURE 7 Polishing direction relationships for samples whose measurements are reported in text (SEE PAGE 280)

tilt preference results in either a positive or negative tilt in an activated state. By observing the behavior of the $\pm 45°$ optical channels as a function of voltage, it is easy to deduce the tilt direction as a result of the electric and magnetic fields applied. The responses of these optical channels are shown in Figure 8 for the case of an electric field applied to a twisted cell. These are just threshold curves and it can be seen that very different curves result for the $\pm 45°$ observations and thus the orientation of the tilt may easily be determined. In fact, the very large distinctions between such $\pm 45°$ observations leads to some possible display and optical memory applications.

That the effective tilt preference is small can be seen from the results of magnetic-field-only experiments where the response of the "preferred" photodiode is monitored as a function of magnetic field but with the magnetic field orientation as a parameter. These are shown in Figures 9 and 10. Again, as for all the experimental observations to be reported here, a twisted cell is monitored and we see that as the magnetic field varies from 0° to 5° in a direction to aid the preferred tilt, little effect is observed. However for orientations *opposing* the tilt preference by as little as 0.5°, definite changes are noticed and by the time a deviation of 1.25° is obtained, the behavior now has assumed a definite non-preferred orientation characteristic as in Figure 8. The conclusion is, for these cells, that an average preferred tilt of about 0.75° exists at

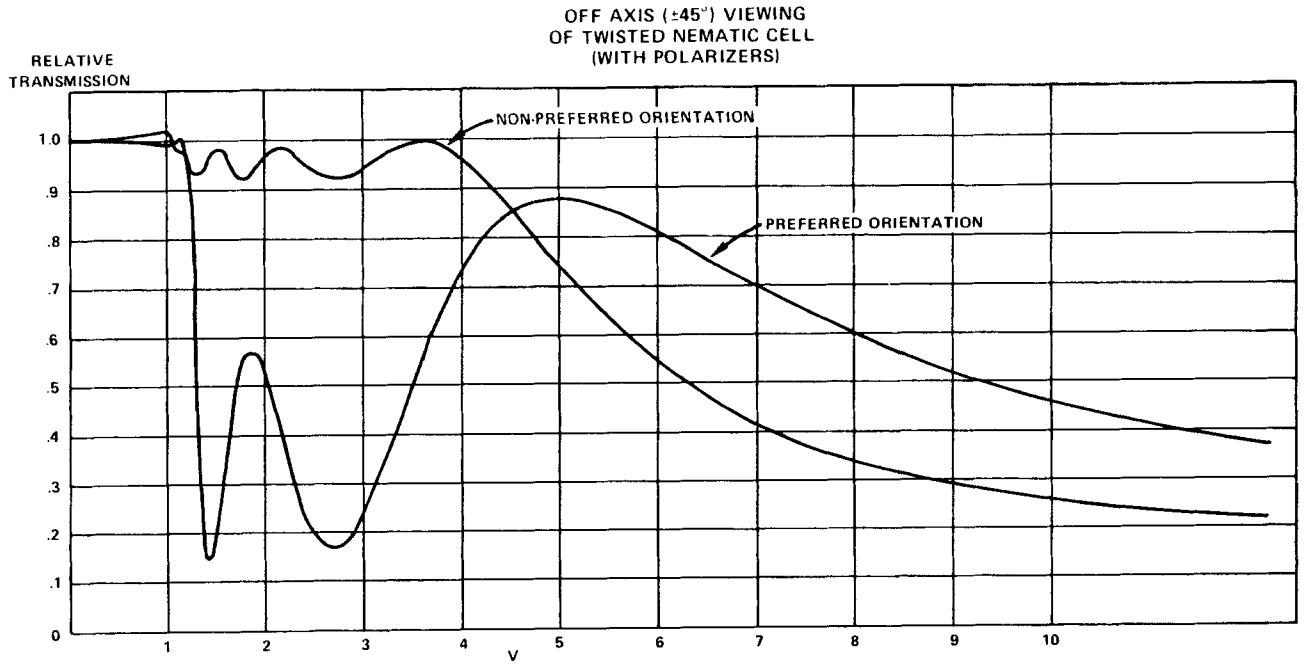

FIGURE 8 Transmission vs. voltage curves for light propagating at 45° to the normal of the cell and either along or off axis with the preferred orientation.

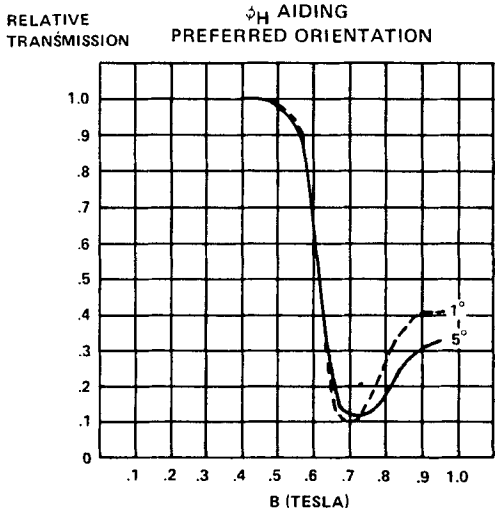

FIGURE 9 Transmission vs. B curves for light transmitted at +45° (preferred orientation direction) for various angles of B which generally enforce the preferred orientation behavior.

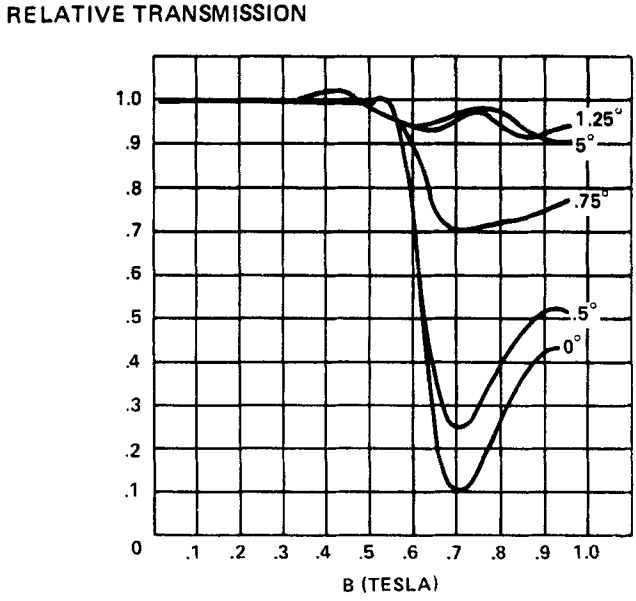

FIGURE 10 Transmission vs. B curves as in Figure 9 but with orientation of B tending to oppose the preferred orientation.

the surface and if the magnetic field is applied off normal by just this amount, then almost no preference exists and either positive or negative tilts may result.

An *average* tilt, $\langle \delta\theta \rangle$, is described because variations over the surface can be expected to give local surface tilts that vary about this average with the result that in certain areas a positive tilt will occur while in others a negative tilt will result—i.e., domains will be formed. Since the LED-Photodiode pairs are observing a finite portion of the surface, a response which varies in proportion to the relative areal occurrence of + or − tilt domains will result. This will be utilized later to define a surface distribution function and a surface tilt probability function which will allow a quantitative description of the surface.

In the case previously described, the spread of $\delta\theta$ about $\langle \delta\theta \rangle$ is evidently small since, as observed above, a variation of 0.5° above and below this $\langle \delta\theta \rangle$ gives preferred or non-preferred behavior over the entire observed region.

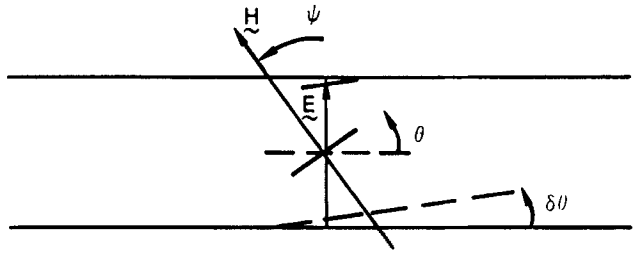

FIGURE 11 Angular relations used in derivation presented in text.

Although the above experiment is readily interpreted, precise measurements are difficult because of the very small angles involved and the uncertainties of the mechanical and magnetic orientations. A much more controllable experiment utilizes the combination of electric and magnetic fields illustrated in Figure 11. Experimentally, the magnetic field is first applied and time is allowed for equilibrium to be attained. The magnetic field is applied at an angle ψ which is fixed and opposes the preferred tilt. The magnetic field intensity is insufficient to attain magnetic threshold but *is* contributing a torque on the liquid crystal molecules which opposes the effects of the built-in preferred tilt. Subsequent application of an above-threshold electric field then will cause preferred or non-preferred tilt as determined by the strength and angle of the magnetic field. The threshold behavior of such an experimental arrangement may be calculated and, for completeness, both the non-twisted and twisted cell will be treated.

THEORY—NON-TWISTED CELL

Using the definitions as described in Figure 11 we write the free energy terms due to elastic forces following Frank's[2] definitions as

$$g_{\mathbf{n}} = \tfrac{1}{2}\{k_{11}(\nabla \cdot \mathbf{n})^2 + k_{22}(\mathbf{n} \cdot \nabla x\mathbf{n})^2 + k_{33}[(\mathbf{n} \cdot \nabla)\mathbf{n}]^2\}$$

where $\mathbf{n}$ is the director axis. In our case

$$\mathbf{n} = \cos\theta\hat{\mathbf{x}} + \sin\theta\hat{\mathbf{z}}$$

and $g_{\mathbf{n}}$ reduces to

$$g_{\mathbf{n}} = \tfrac{1}{2}\{k_{11}\cos^2\theta + k_{33}\sin^2\theta\}\theta_z^2.$$

The electric free energy is obtained from†

$$g_{\mathbf{E}} = -\tfrac{1}{2}\mathbf{P} \cdot \mathbf{E}$$

where $\mathbf{P}$ is the induced polarization and, in terms of the macroscopic susceptibility components, can be written in terms of $\mathbf{E}$ and $\mathbf{n}$ as

$$\mathbf{P} = \varepsilon_0[\chi_\perp \mathbf{E} + \Delta\chi(\mathbf{n} \cdot \mathbf{E})\mathbf{n}]$$

where $\Delta\chi \equiv \chi_{\parallel} - \chi_\perp$ and $\chi_{\parallel}$ and $\chi_\perp$ are the electric susceptibility components parallel and perpendicular to the director axis respectively. Therefore we have, except for terms not involving $\mathbf{n}$ and using $\varepsilon_0(1 + \chi) = \varepsilon$,

$$g_{\mathbf{E}} = -\frac{\varepsilon_0 \Delta\chi}{2}(\mathbf{n} \cdot \mathbf{E})^2 = -\frac{\Delta\varepsilon}{2}(\mathbf{n} \cdot \mathbf{E})^2.$$

Similarly we have (letting χ now be the *magnetic* susceptibility)

$$g_{\mathbf{H}} = -\frac{\mu_0}{2}\mathbf{M} \cdot \mathbf{H}$$

where

$$\mathbf{M} = \chi_\perp \mathbf{H} + \Delta\chi(\mathbf{n} \cdot \mathbf{H})\mathbf{n}$$

and thus (using $\mu = \mu_0(1 + \chi)$)

$$g_{\mathbf{H}} = \frac{-\mu_0}{2}\Delta\chi(\mathbf{n} \cdot \mathbf{H})^2 = -\tfrac{1}{2}\Delta\mu(\mathbf{n} \cdot \mathbf{H})^2.$$

So finally, in terms of θ we have for the total free energy density,

$$g = \tfrac{1}{2}\{k_{11}\cos^2\theta + k_{33}\sin^2\theta\}\theta_z^2 - \frac{\Delta\varepsilon}{2}E^2\sin^2\theta - \frac{\Delta\mu}{2}H^2\sin^2(\theta - \psi).$$

† SI units are used throughout.

In order that $\theta(z)$ should bring $G = \int g \, dV$ to a minimum, the Euler–Lagrange equation

$$\frac{\partial g}{\partial \theta} - \frac{\partial}{\partial z}\left(\frac{\partial g}{\partial \theta_z}\right) = 0$$

must be satisfied. This leads to the differential equation

$$(k_{11}\cos^2\theta + k_{33}\sin^2\theta)\theta_{zz} = -\Delta\varepsilon E^2 \sin\theta\cos\theta - \Delta\mu H^2 \sin(\theta - \psi)\cos(\theta - \psi).$$

Since we are interested in threshold and sub-threshold behavior we now make the small angle approximation and keep only first order terms in θ.

Then we find

$$k_{11}\theta_{zz} = -\Delta\varepsilon E^2\theta - \Delta\mu H^2\left[\theta\cos(2\psi) - \frac{\sin(2\psi)}{2}\right]$$

or

$$\theta_{zz} = -\left[\frac{\Delta\varepsilon E^2}{k_{11}} + \frac{\Delta\mu H^2}{k_{11}}\cos(2\psi)\right]\theta + \frac{\Delta\mu H^2}{2}\sin(2\psi)$$

Now it is convenient to transform this equation into a dimensionless form which allows for a simpler form and is more readily interpreted. The following variable changes are made and the corresponding normalized variable will be denoted by a circumflex:

$$\theta \to \hat{\theta} \equiv \frac{\theta}{\delta\theta}$$

$$E^2 \to \hat{V}^2 \equiv \frac{V^2}{V_T} = \frac{E^2}{E_T}$$

$$H^2 \to \hat{H}^2 \equiv \frac{H^2}{H_T}$$

$$Z \to u \equiv \frac{Z}{L}, \quad -\tfrac{1}{2} \le u \le \tfrac{1}{2}$$

where we utilize the known relations

$$\frac{\Delta\varepsilon}{k_{11}} = \left(\frac{\pi}{L}\right)^2 \frac{1}{E_T^2}$$

$$\frac{\Delta\mu}{k_{11}} = \left(\frac{\pi}{L}\right)^2 \frac{1}{H_T^2}$$

for the electric and magnetic threshold fields.

This results finally in

$$\hat{\theta}_{uu} = -\pi^2[\hat{V}^2 + \hat{H}^2\cos(2\psi)]\hat{\theta} + \pi^2\frac{\hat{H}^2}{2\delta\theta}\sin(2\psi)$$

This equation may be solved by noting that a particular solution may be seen to be

$$\hat{\theta}_p = \frac{\frac{\hat{H}^2}{2\delta\theta}\sin(2\psi)}{\hat{V}^2 + \hat{H}^2\cos(2\psi)}$$

On the other hand, solutions of the homogeneous equation are of the form,

$$\hat{\theta}_H = A\sin[\pi[\hat{V}^2 + \hat{H}^2\cos(2\psi)]^{1/2}u] + B\cos[\pi[\hat{V}^2 + \hat{H}^2\cos(2\psi)]^{1/2}u]$$

The general solution, then, is of the form

$$\hat{\theta} = \hat{\theta}_H + \hat{\theta}_P$$

which satisfies the boundary conditions

$$\hat{\theta}_u(0) = 0$$
$$\hat{\theta}(\pm\tfrac{1}{2}) = 1$$

These conditions lead to

$$\hat{\theta}(u) = \frac{\frac{\hat{H}^2}{2\delta\theta}\sin(2\psi)}{\hat{V}^2 + \hat{H}^2\cos(2\psi)} + \left(1 - \frac{\frac{\hat{H}^2}{2\delta\theta}\sin(2\psi)}{\hat{V}^2 + \hat{H}^2\cos(2\psi)}\right) \times \frac{\cos\{\pi[\hat{V}^2 + \hat{H}^2\cos(2\psi)]^{1/2}u\}}{\cos\left\{\frac{\pi}{2}[\hat{V}^2 + \hat{H}^2\cos(2\psi)]^{1/2}\right\}}$$

This equation, resulting as it does from a small angle approximation, may be considered accurate for values of θ up to 10°. Since experimentally we have that $\delta\theta \gtrsim 1°$ for many surfaces, this means the above equation is accurate for $\hat{\theta} \gtrsim 10$.

The threshold behavior of the cell may now be ascertained. Evidently a threshold condition exists for the condition

$$U^2 \equiv \hat{V}^2 + \hat{H}^2\cos(2\psi) \to 1$$

since $\hat{\theta}$ diverges here. The tilt behavior can be deduced from the sign of $\hat{\theta}(u)$ as $U \to 1$. In fact preferred or non-preferred behavior may be determined by the condition

$$1 - \frac{\hat{H}^2}{2\delta\theta}\sin(2\psi)\begin{cases} > 0 & \text{preferred} \\ > 0 & \text{non-preferred} \end{cases}$$

This depends on the magnitude of H, ψ and $\delta\theta$. The above condition may alternatively be expressed as

$$\gamma \sin(2\psi) \begin{cases} < 1 & \text{preferred} \\ > 1 & \text{non-preferred} \end{cases}$$

where

$$\gamma \equiv \frac{\hat{H}^2}{2\delta\theta}.$$

Considerable simplification occurs if we choose, as is the case for all experiments reported here, $\psi = \pi/4$. Then

$$\hat{\theta}(u) = \frac{\gamma}{\hat{V}^2} + \left(1 - \frac{\gamma}{\hat{V}^2}\right) \frac{\cos(\pi \hat{V} u)}{\cos\left(\frac{\pi \hat{V}}{2}\right)}$$

and now the threshold condition is simply $\hat{V} \to 1$; i.e. the electric field threshold for a cell with or without a magnetic field at $\psi = \pi/4$ is unchanged. Some calculated plots of the behavior of this equation are plotted in Figures 12 and 13 for various values of γ and u.

Of interest here is information on the material and processing parameter $\delta\theta$. Experimentally we may apply a magnetic field condition such that $\gamma = 1$. Then, knowing the critical magnetic field we may calculate

$$\delta\theta = \tfrac{1}{2}\hat{H}_c^2$$

or, in degrees,

$$\delta\theta = 28.65\hat{H}_c^2$$

THEORY—TWISTED CELL

An entirely similar procedure may be used for the twisted cell, although the complexity is increased and, in order to obtain an analytical form for the threshold behavior, further simplifications must be made. These further simplifications do not have a strong influence on the behavior, however, and the resulting equations may again be assumed to be fairly accurate.

In the twisted cell, a further degree of freedom is added in that a twist angle, ϕ, is introduced. Assuming the same geometry as for the non-twisted cell, we now add the boundary conditions.

$$\phi(-L/2) = -\pi/4$$
$$\phi(L/2) = \pi/4$$

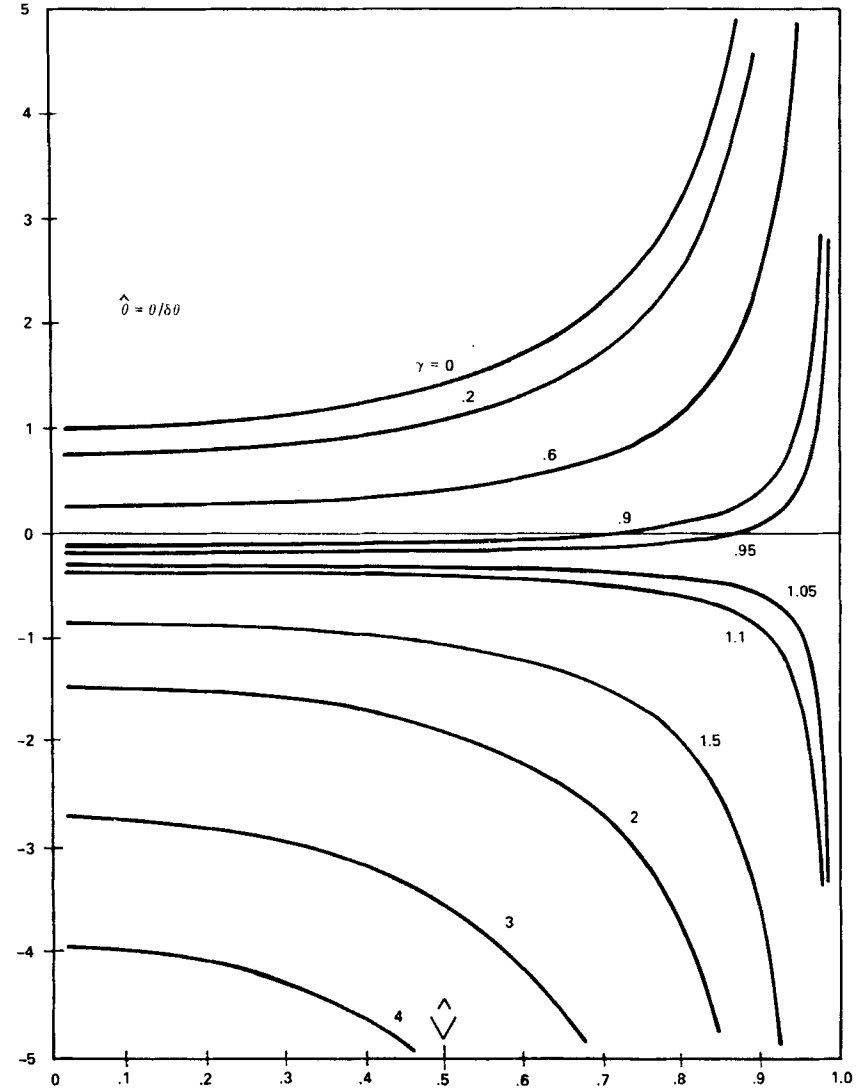

FIGURE 12 Central molecule orientation as a function of voltage (normalized) for various strengths of the magnetic bias.

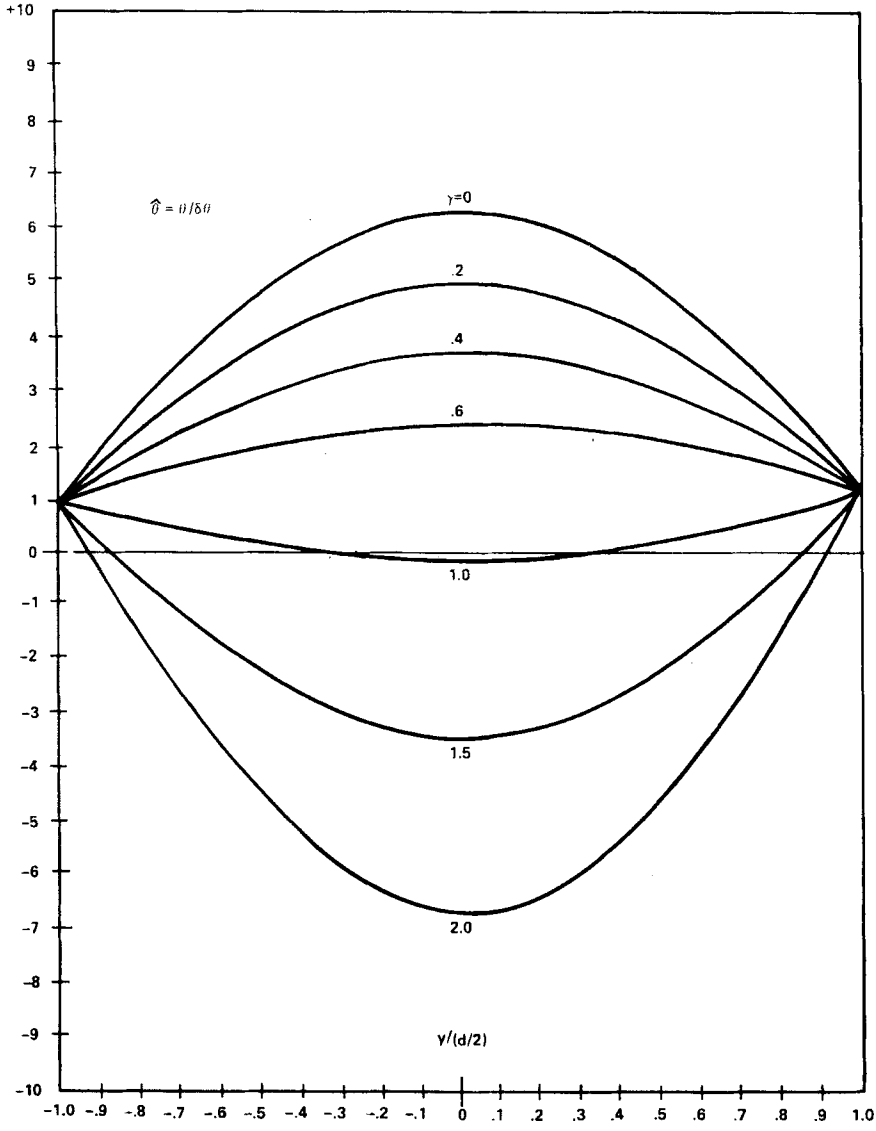

FIGURE 13 Molecular orientation distribution at $\hat{V} = 0.9$ and various γ values.

giving a 90° twist as a whole. Now we have

$$\mathbf{n} = \cos\theta\cos\phi\hat{\mathbf{x}} + \cos\theta\sin\phi\hat{\mathbf{y}} + \sin\theta\hat{\mathbf{z}}.$$

The resulting elastic, electric and magnetic free energies are:

Elastic

$$g_{\mathbf{n}} = \tfrac{1}{2}[(k_{11}\cos^2\theta + k_{33}\sin^2\theta)\theta_z^2 + (k_{22}\cos^2\theta + k_{33}\sin^2\theta)\cos^2\theta\phi_z^2]$$

Electric

$$g_{\mathbf{E}} = -\frac{\Delta\varepsilon}{2}E^2\sin^2\theta$$

Magnetic

$$g_{\mathbf{H}} = -\frac{\Delta\mu H^2}{2}(\cos^2\psi\sin^2\theta + \sin^2\psi\cos^2\phi\cos^2\theta - 2\sin\psi\cos\psi\cos\theta\sin\theta\cos\phi).$$

Utilization of these equations in the Euler-Lagrange criteria results in two coupled differential equations which are:

$$\begin{aligned}&(k_{11}\cos^2\theta + k_{33}\sin^2\theta)\theta_{zz} + 2(k_{33} - k_{11})\sin\theta\cos\theta\theta_z^2\\ &\quad - (k_{33} - k_{22})\sin\theta\cos^3\theta\phi_z^2 + (k_{22}\cos^2\theta + k_{33}\sin^2\theta)\cos\theta\sin\theta\phi_z^2\\ &\quad + \Delta\varepsilon E^2\sin\theta\cos\theta + \Delta\mu H^2[\cos(2\psi)\sin\theta\cos\theta\\ &\quad + \sin^2\psi\sin^2\phi\sin\theta\cos\theta - \sin\psi\cos\psi\cos\phi\cos(2\theta)] = 0\end{aligned}$$

and

$$\begin{aligned}&(k_{22}\cos^2\theta + k_{33}\sin^2\theta)\cos^2\theta\phi_{zz} + 4(k_{33} - k_{22})\sin\theta\cos^3\theta\theta_z\phi_z\\ &\quad - 2k_{33}\sin\theta\cos\theta\theta_z\phi_z - \Delta\mu H^2(\sin^2\psi\sin\phi\cos\phi\cos^2\theta\\ &\quad - \sin\psi\cos\psi\sin\phi\cos\theta\sin\theta) = 0\end{aligned}$$

Now, again the small angle approximation is made and the above reduce to:

$$\begin{aligned}&k_{11}\theta_{zz} + (2k_{22} - k_{33})\phi_z^2\theta + \Delta\varepsilon E^2\theta\\ &\quad + \Delta\mu H^2[\cos(2\psi)\theta + \sin^2\psi\sin^2\phi\theta - \sin\psi\cos\psi\cos\phi] = 0\end{aligned}$$

$$k_{22}\phi_{zz} - \Delta\mu H^2(\sin^2\psi\sin\phi\cos\phi - \sin\psi\cos\psi\sin\phi\theta) = 0$$

Without further simplification, numerical procedures would be indicated for the solutions of these coupled equations. However, a highly accurate solution may be obtained if we assume $\phi(Z)$ is essentially undisturbed by the magnetic and electric fields. In this case we have

$$\phi(Z) \simeq \frac{\pi Z}{2L}$$

and, as we shall see, a solution may then be obtained. An estimate of the accuracy of this assumption may be ascertained if we search for a solution for $\phi(Z)$ of the form

$$\phi(Z) = \frac{\pi Z}{2L} + \delta\phi$$

Substitution of this into the second differential equation, remembering that both θ and $\delta\phi$ are small, using $\psi = \pi/4$ and applying boundary conditions leads to

$$\delta\phi(Z) = \tfrac{1}{8}\hat{H}^2\left[2\frac{Z}{L} - \sin\left(\pi\frac{Z}{L}\right)\right]$$

where

$$\hat{H}^2 \equiv \left(\frac{H}{H_T}\right)^2$$

$$H_T^2 \equiv \left(\frac{\pi}{L}\right)^2 \frac{k_{22}}{\Delta\mu}$$

$\delta\phi(Z)$ has a maximum deviation for $Z \simeq 0.377$ L and this results in

$$\delta\phi_{\max} = -0.0215\,\hat{H}^2.$$

Now, even if $\hat{H}^2 = 1$, the maximum deviation is only of the order of $-1°$ which may be ignored. In all of our experiments, small values of $\hat{H}$ are used, consequently we may, with high accuracy assume $\phi = (\pi/2)(Z/L)$.

The first differential equation becomes now

$$\theta_{zz} = -\left[\frac{(2k_{22} - k_{33})\phi_z^2}{k_{11}} + \frac{\Delta\varepsilon E^2}{k_{11}} + \frac{\Delta\mu H^2}{k_{11}}\{\cos(2\psi) + \sin^2\psi\sin^2\phi\}\right]\theta$$

$$+ \frac{\Delta\mu H^2}{2k_{11}}\sin(2\psi)\cos\phi$$

Making a transformation of variables to a dimensionless form, as in the non-twisted case, we arrive at

$$\hat{\theta}_{uu} = -\pi^2[(1-\lambda) + \lambda\hat{V}^2 + \lambda\hat{H}^2\{\cos(2\psi) + \sin^2\psi\sin^2\phi\}]\theta$$

$$+ \pi^2\frac{\lambda\hat{H}^2}{2\delta\theta}\sin(2\psi)\cos\phi$$

where we have used the expressions for the twisted cell threshold fields[3]

$$E_T^2 \equiv \left(\frac{\pi}{L}\right)^2 \frac{k_{11}}{\Delta\varepsilon}\lambda$$

$$H_T^2 \equiv \left(\frac{\pi}{L}\right)^2 \frac{k_{11}}{\Delta\mu}\lambda$$

and

$$\lambda \equiv \left[1 - \left(\frac{L}{\pi}\right)^2 \left(\frac{2k_{22} - k_{33}}{k_{11}}\right)\phi_z^2\right]$$

Finally, we now further assume that the term

$$\lambda\hat{H}^2[\cos(2\psi) + \sin^2\psi \sin^2\phi] \ll \lambda\hat{V}^2$$

(especially near threshold where $\hat{V} \to 1$). In fact, our experiments utilize $\psi = \pi/4$ and $\hat{H}^2 \lesssim 0.04$. Utilizing $\phi_{\max} = \pi/4$, albeit at the boundary, we have

$$0.01\,\lambda \ll \lambda$$

which certainly justifies the assumption as $\hat{V} \to 1$. Therefore, with $\psi = \pi/4$, we finally have

$$\hat{\theta}_{uu} = -\pi^2[(1 - \lambda) + \lambda\hat{V}^2]\theta + \pi^2\lambda \frac{\hat{H}^2}{2\delta\theta}\cos\left(\frac{\pi u}{2}\right)$$

proceeding as for the non-twisted cell we find a particular solution is

$$\hat{\theta}_p = \frac{\lambda H^2}{2\delta\theta} \frac{\cos\left(\frac{\pi u}{2}\right)}{\lambda(\hat{V}^2 - 1) + \frac{3}{4}}$$

while the homogeneous solution is of the form

$$\hat{\theta}_H = A\cos(\pi[\lambda(\hat{V}^2 - 1) + 1]^{1/2}u) + B\sin(\pi[\lambda(\hat{V}^2 - 1) + 1]^{1/2}u).$$

Applying the boundary conditions to the general solution then leads to the result

$$\hat{\theta}(u) = \frac{\frac{\lambda\hat{H}^2}{2\delta\theta}\cos\frac{\pi}{4}}{\lambda(\hat{V}^2 - 1) + \frac{3}{4}}\cos\left(\frac{\pi u}{2}\right) + \left[1 - \frac{\frac{\lambda\hat{H}^2}{2\delta\theta}\cos\frac{\pi}{4}}{\lambda(\hat{V}^2 - 1) + \frac{3}{4}}\right]\frac{\cos(\pi[\lambda(\hat{V}^2 - 1) + 1]^{1/2}u)}{\cos(\pi/2[\lambda(\hat{V}^2 - 1) + 1]^{1/2})}$$

Again we see that the threshold condition for this twisted cell with both magnetic and electric fields applied is just the condition $\hat{V} \to 1$, i.e. the same condition as for a cell with no magnetic field applied.

As for the non-twisted cell, we deduce the following criteria for preferred or non-preferred behavior:

$$\tfrac{4}{3}\lambda \frac{\hat{H}^2}{2\delta\theta} \cos\frac{\pi}{4} \begin{cases} <1 & \text{preferred tilt} \\ >1 & \text{non-preferred tilt} \end{cases}$$

A critical field may then be calculated; it is

$$\hat{H}_c^2 = \frac{3}{2\cos(\pi/4)} \lambda\delta\theta \simeq 2.12\lambda\delta\theta$$

Alternatively, if $\hat{H}_c$ is experimentally determined, we then have

$$\delta\theta = \frac{2\cos(\pi/4)}{3\lambda} \hat{H}_c^2 \simeq \frac{\hat{H}_c^2}{2.12\lambda}$$

These results for the twisted cell may be compared with those of the non-twisted cell. In the non-twisted case, an unambiguous calculation of $\delta\theta$ from $\hat{H}_c$ may be made. Unfortunately, in the twisted case, the term λ must also be known. The simplest definition for λ is

$$H_T(\text{twisted}) = \lambda H_T(\text{non-twisted})$$

and generally $\lambda \lesssim 1$. If λ is known, either through its definition in terms of fundamental parameters or from experimental determination of twisted and non-twisted threshold fields, then $\delta\theta$ may be calculated.

SUMMARY

Summarizing, we have seen that for the non-twisted cell, with a magnetic field applied at $\psi = \pi/4$ and opposing the preferred tilt direction that the director orientation may be described by

$$\hat{\theta}(u) = \frac{\gamma}{\hat{V}^2} + \left(1 - \frac{\gamma}{\hat{V}^2}\right) \frac{\cos(\pi\hat{V}u)}{\cos(\pi\hat{V}/2)}$$

where $\hat{\theta} = \theta/\delta\theta$, $u = Z/L$, $\hat{V} = V/V_T$ and $\gamma \equiv \hat{H}^2/2\delta\theta$ with $\hat{H} = H/H_T$.

A critical magnetic field strength can be defined such that non-preferred tilt will occur under application of a threshold electric fiedl ($\hat{V} \to 1$) and is given by

$$\hat{H}_c^2 = 2\delta\theta$$

Alternatively, knowing the critical field, $\delta\theta$ may be calculated from

$$\delta\theta = \tfrac{1}{2}\hat{H}_c^2$$

In the case of the twisted cell we have,

$$\phi = \frac{\pi u}{2}$$

$$\hat{\theta} = \frac{\lambda\gamma \cos(\pi/4)}{\lambda(\hat{V}^2 - 1) + \frac{3}{4}} \cos(\pi u/2) + \left[1 - \frac{\lambda\gamma \cos(\pi/4)}{\lambda(\hat{V}^2 - 1) + \frac{3}{4}}\right] \frac{\cos(\pi[\lambda(\hat{V}^2 - 1) + 1]^{1/2} u)}{\cos\left(\frac{\pi}{2}[\lambda(\hat{V}^2 - 1) + 1]^{1/2}\right)}$$

$$\hat{H}_c^2 = \frac{3}{2\cos(\pi/4)} \lambda\delta\theta \simeq 2.12\lambda\delta\theta$$

$$\delta\theta = \frac{2\cos(\pi/4)}{3\lambda} \hat{H}_c^2 \simeq \frac{\hat{H}_c^2}{2.12\lambda}$$

EXPERIMENTAL

The preceding relationships between the critical magnetic field to induce non-preferred tilt, and the effective surface tilt, $\delta\theta$, have been applied to various twisted cells to determine the magnitudes of $\delta\theta$ and constancy of $\delta\theta$ over the surfaces of cells. Various surface treatments have also been compared to determine the effects of surface treatments on bonding properties.

Unfortunately, all measurements were performed on twisted cells whose λ value is unknown. Nevertheless, in all the experiments reported here, the same liquid crystal was used and surface conditions were changed. Consequently λ is constant in these experiments and the representative angle for $\delta\theta$,

$$\delta\theta = \frac{H_c^2}{2}$$

is reported which, although strictly true only for the non-twisted cell, is nevertheless a representative value assuming $\lambda \simeq 1$. Primarily it is the technique, underlying theory and representative applications which is being reported.

SURFACE TILT PROBABILITY AND DISTRIBUTION FUNCTIONS

An experimental technique has been developed which utilizes the apparatus and field configurations of Figure 6 to determine the magnitude and spread of the surface tilt. In this technique, the magnetic field is oriented at an angle $\psi = \pi/4$ (in the opposing direction) because this maximizes the coupling and also simplifies the equations.

If the magnetic field is zero, Figure 8 depicts the type of transmission behavior observed at the $\pm 45°$ channels (we will arbitrarily call the $+45°$ channel the preferred channel and choose electronic signal levels as positive for high extinction and negative for high transmission). Consequently, we see that, for this liquid crystal, at an applied voltage of approximately 1.4 or 2.7 volts, a large contrast exists between the preferred and non-preferred channels with the $+45°$ giving a positive output and the $-45°$ channel a negative output. A voltage of 2.7 volts was chosen for observation of tilt preferences because of its large constrast and higher speed of operation.

Now, if the cell is deactivated and then allowed to come into equilibrium with some non-zero, opposing magnetic field, the tilt preference will be affected by the magnetic field. If the field strength considerably exceeds the critical field, H_c, then the tilt preference will reverse and subsequent application of the "read" voltage will result in observation of non-preferred behavior--i.e., the $+45°$ channel will be negative indicating high transmission and the $-45°$ channel will be positive indicating high extinction. By repeating this process—deactivate cell, change magnetic field strength and allow equilibrium to be obtained (a few seconds), activate cell and measure $\pm 45°$ channel signal voltages—the ideal curve of Figure 14 could be expected.

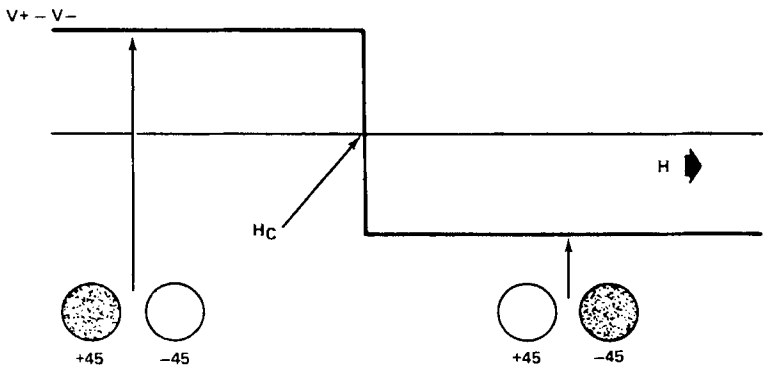

FIGURE 14 Idealized voltage differences between the preferred and non-preferred channels as a function of the magnetic field. Also shown are the visual appearances of finite portions of the cell when viewed in the $+45°$ and $-45°$ directions.

What is plotted is the difference in voltages between the $\pm 45°$ channels ($V_+ - V_-$) versus the applied magnetic field. Also indicated are representations of the view through the $\pm 45°$ channels. Hc can be determined by such a curve and consequently $\delta\theta$.

This curve is idealized because in reality a finite area of the surface is being observed by the LED-photodiode pairs and variations in $\delta\theta$ exist over the surface. In our experiments, a region of about 3mm diameter was observed. This means that as H approaches the critical field strengths, some regions with slightly smaller tilt preferences may "flip" earlier than other regions with stronger tilt preferences. The result is that in the critical field region, a mottly appearance will result because of numerous small domains of negative tilt surrounded by positive tilt regions. Figure 15 illustrates this more realistic situation with indications of the sample appearance at various portions of the critical field strength region. It should be noted that the two views will be exact contrast opposites. Also, the square of the applied magnetic field is plotted since, for any region which has flipped, $\delta\theta \alpha H^2$.

The $V_+ - V_-$ signals essentially indicate the area of the viewed region which have preferred tilt. By appropriate electronic scaling, a signal P_+ was con-

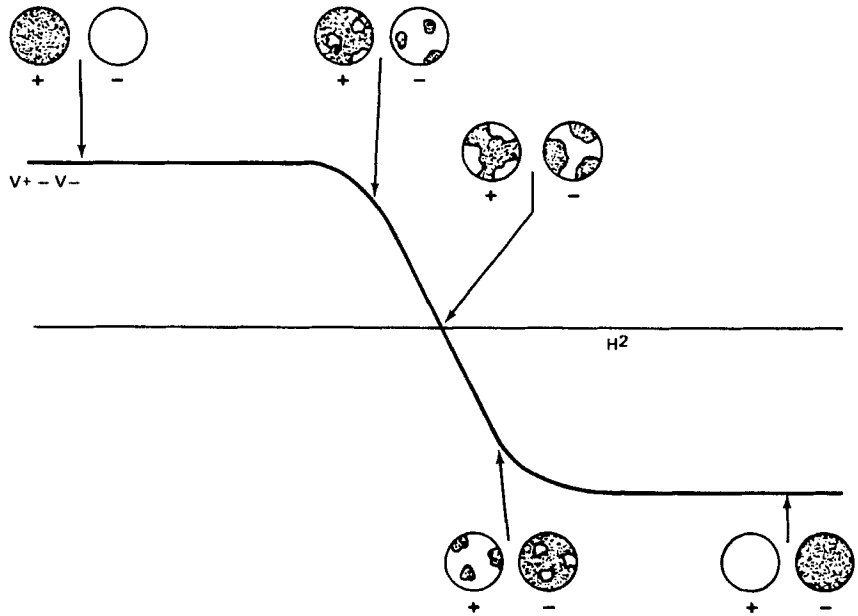

FIGURE 15 Presentation similar to that of Figure 14 except a realistic sample with surface tilt preferences which varies spatially on the sample surface is depicted. Also, H^2 is used as the abcissa instead of H since surface tilt is proportional to H^2.

structed which lies between 0 and 1 with the property that P_+ represents the fraction of the area of the sample (in view) which has positive or preferred tilt. In addition, by previous measurements we determine H_T for the device under test. This allows us to scale the abcissa of our curves directly in terms of a surface tilt, θ_s, by the relation

$$\theta_s = \tfrac{1}{2}\hat{H}^2$$

Experimentally, electronic squaring circuits may be used to allow direct plotting of $P_+(\theta_s)$ versus θ_s.

Now, this signal $P_+(\theta_s)$ may in turn be further defined in terms of a surface tilt distribution function, $f(\theta_s)$, as

$$P_+(\theta_s) \equiv 1 - \int_{-\pi/2}^{\theta_s} f(\theta_s)\, d\theta_s \qquad -\pi/2 < \theta_s < \pi/2$$

where $f(\theta_s)$ denotes the fraction of the area whose surface tilt lies between θ_s and $\theta_s + d\theta_s$. $P_+(\theta_s)$ is actually then the surface tilt probability function being the fraction of the area whose tilts are *greater* than θ_s. Note therefore that

$$f(\theta_s) = -\frac{\partial P_+}{\partial \theta_s}$$

or in terms of $P_+(H)$,

$$f(\theta_s) = -\left(\frac{\partial P_+}{\partial \hat{H}}\right)\left(\frac{\partial \hat{H}}{\partial \theta_s}\right)$$

But

$$\hat{H} = (2\theta_s)^{1/2}$$

therefore

$$\frac{\partial \hat{H}}{\partial \theta_s} = \frac{1}{\hat{H}}$$

and

$$f(\theta_s) = -\hat{H}^{-1}\frac{\partial P_+}{\partial \hat{H}}$$

Figure 16 illustrates the expected behavior and relations.

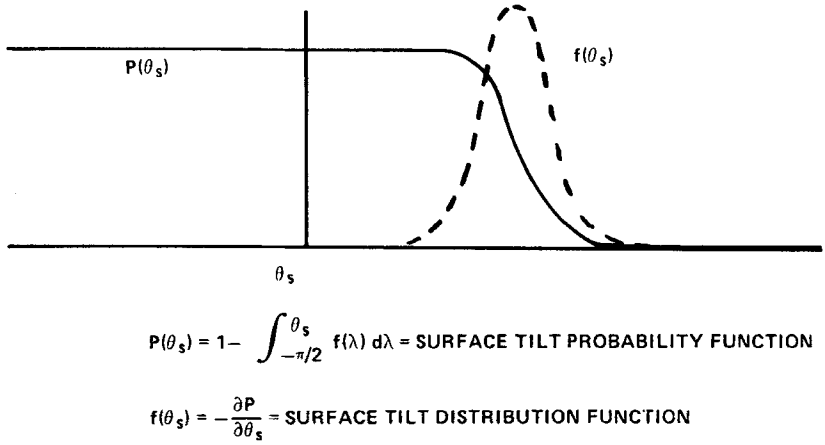

FIGURE 16 Surface tilt probability function and its related distribution function $f(\theta_s)$.

EXPERIMENTAL

Gaussian distribution

In most cases of a well-prepared surface, a Gaussian distribution can be assumed. That this is the case can be seen from a comparison between the Gaussian assumption and actual measurement of $f(\theta_s)$ by graphical means from a plot of $P_+(\theta_s)$. A Gaussian distribution for $f(\theta_s)$ assumes that

$$f_G(\theta_s) = \frac{1}{(2\pi\sigma^2)^{1/2}} \exp[-(\theta_s - \langle\theta\rangle_s)^2/2\sigma^2]$$

$$\sigma \equiv (\langle\theta_s^2\rangle - \langle\theta_s\rangle^2)^{1/2}$$

where it is assumed that $-\infty < \theta_s < \infty$, although $f(\theta_s) = 0$ for $|\theta_s| > \pi/2$. This is a fair assumption since small values of θ_s are experienced. With this $f(\theta_s)$ then, $P_+(\theta_s)$ can be expressed in terms of the error functions. Through consideration of this resulting expression we find that $P_+(\langle\theta_s\rangle) = 0.5$ while $P_+(\theta_s^*) = 0.25$ or 0.75 for θ_s^* satisfying

$$|\theta_s^* - \langle\theta_s\rangle| = 0.48\sqrt{2}\sigma$$

Consequently from a plot of $P_+(\theta_s)$, $\langle\theta_s\rangle$ and θ_s^* may be obtained yielding

$$\sigma = 1.47|\theta_s^* - \langle\theta_s\rangle|$$

fully determining $f_G(\theta_s)$.

In Figure 17, $P_+(\theta_s)$ is shown while Figure 18 shows the resulting measured and calculated distributions. The agreement is reasonably good.

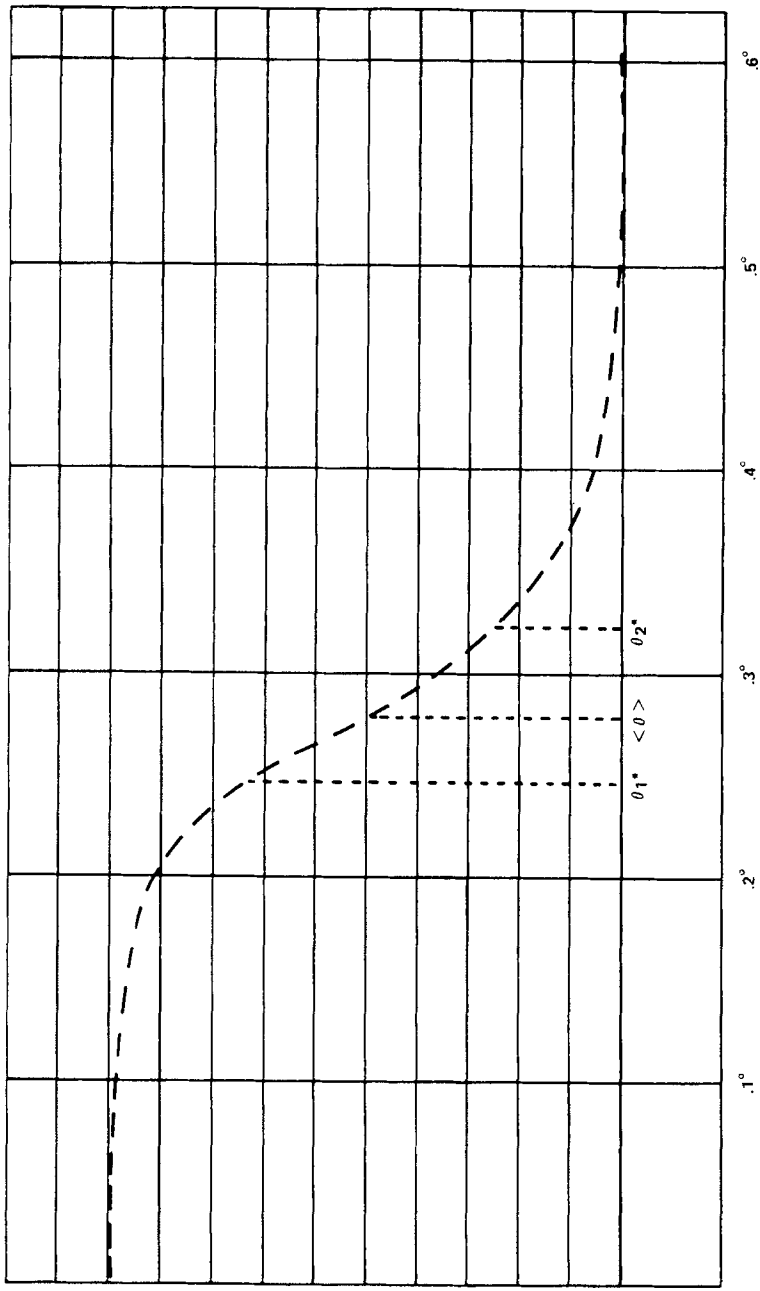

FIGURE 17 Measured surface tilt probability function for a representative surface.

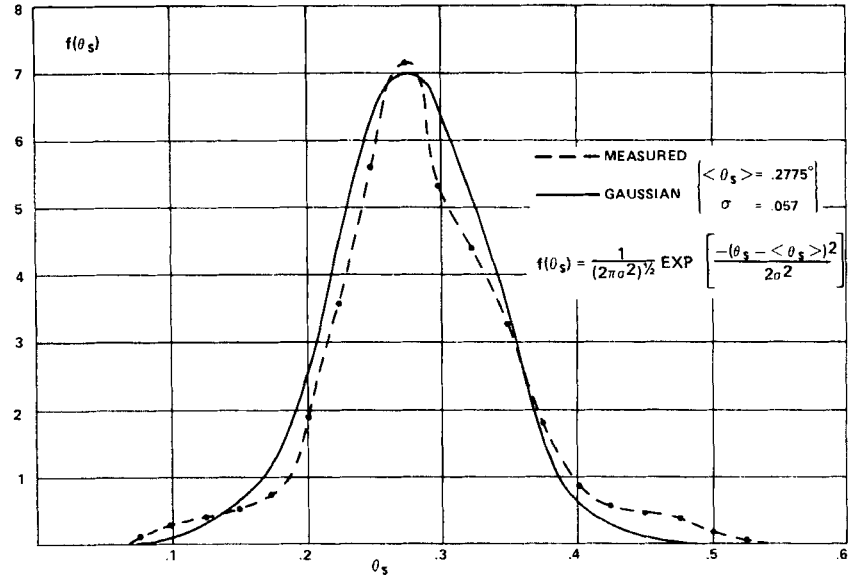

FIGURE 18 Measured distribution function as determined from obtaining graphical derivatives of the probability function of Figure 17. Comparison is made to a Gaussian distribution deduced from fitting to Figure 17.

Non-Gaussian surfaces

That a Gaussian distribution cannot always be assumed is shown in Figures 19 and 20 where a very poor (dirty) cell was analyzed graphically from $P_+(\theta_s)$. A good cell, however, usually has the symmetric shape of a Gaussian distribution and for most of our work has been assumed as such.

Effects of surface type and preparation

Figure 21 represents results of measurements performed on samples fabricated with a variety of techniques. All samples utilized the same liquid crystal, a proprietary all-ester liquid crystal WT-1, and therefore the resulting differences reflect variations in surface conditions. The curves indicated are representative curves; a given technique will consistently yield results very close to the representative curves shown.

The curve marked "Diamond" represents sample cells fabricated with SiO_2 covered electrodes which were polished in the proper directions with 0.5μ diamond paste on a felt cloth. Subsequently the cells were cleaned and assembled. Notice the very sharp distribution but unfortunately small value of $\langle\theta_s\rangle$. In fact, some portions of the surface have negative θ_s values and this implies the occurrence of tilt domains in an ordinary cell.

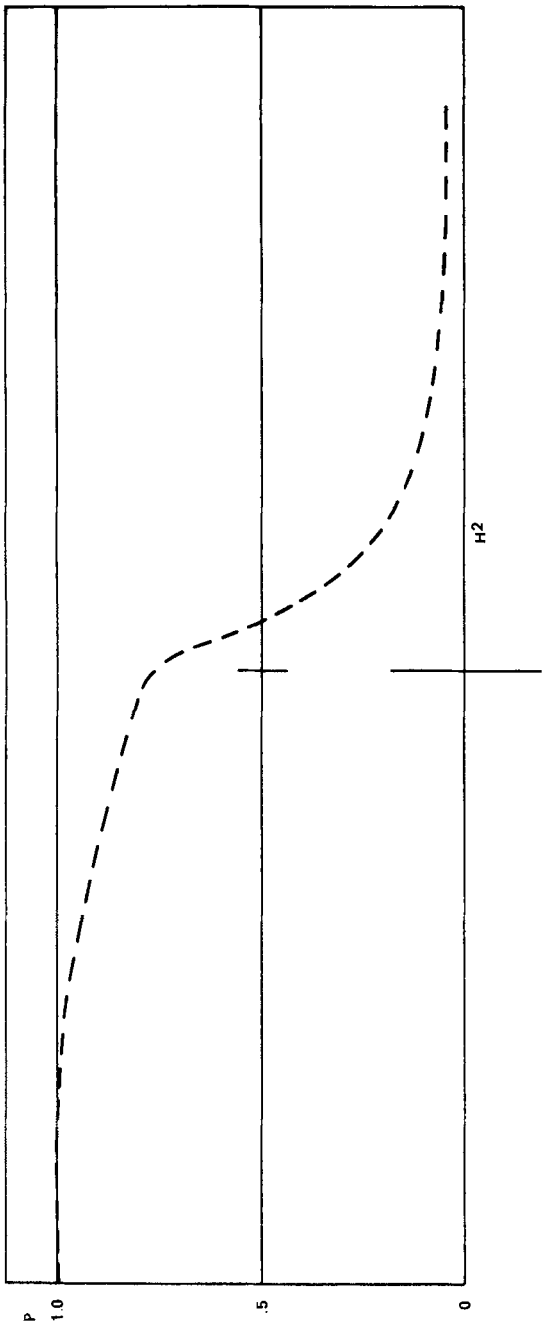

FIGURE 19 Measured probability function for a poor surface.

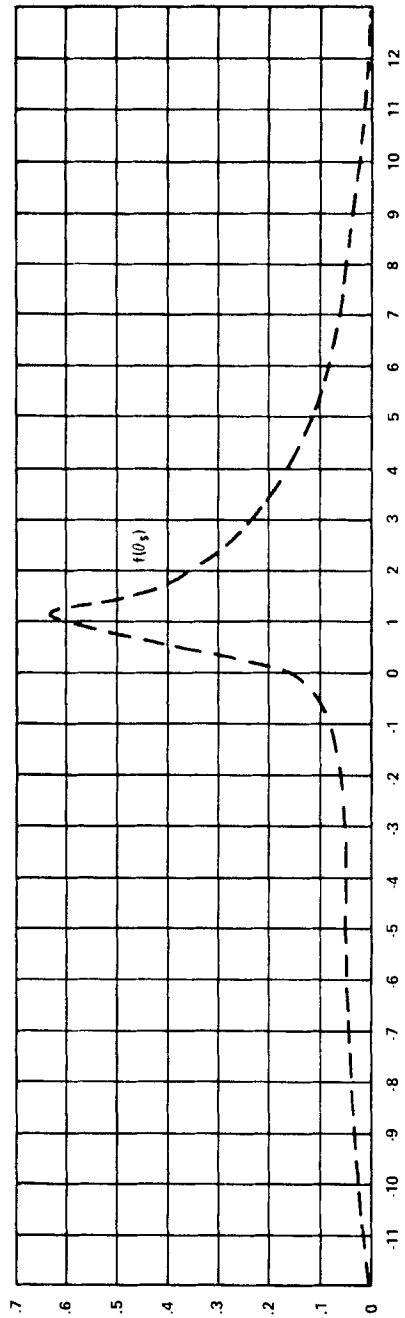

FIGURE 20 Distribution function for surface of Figure 19.

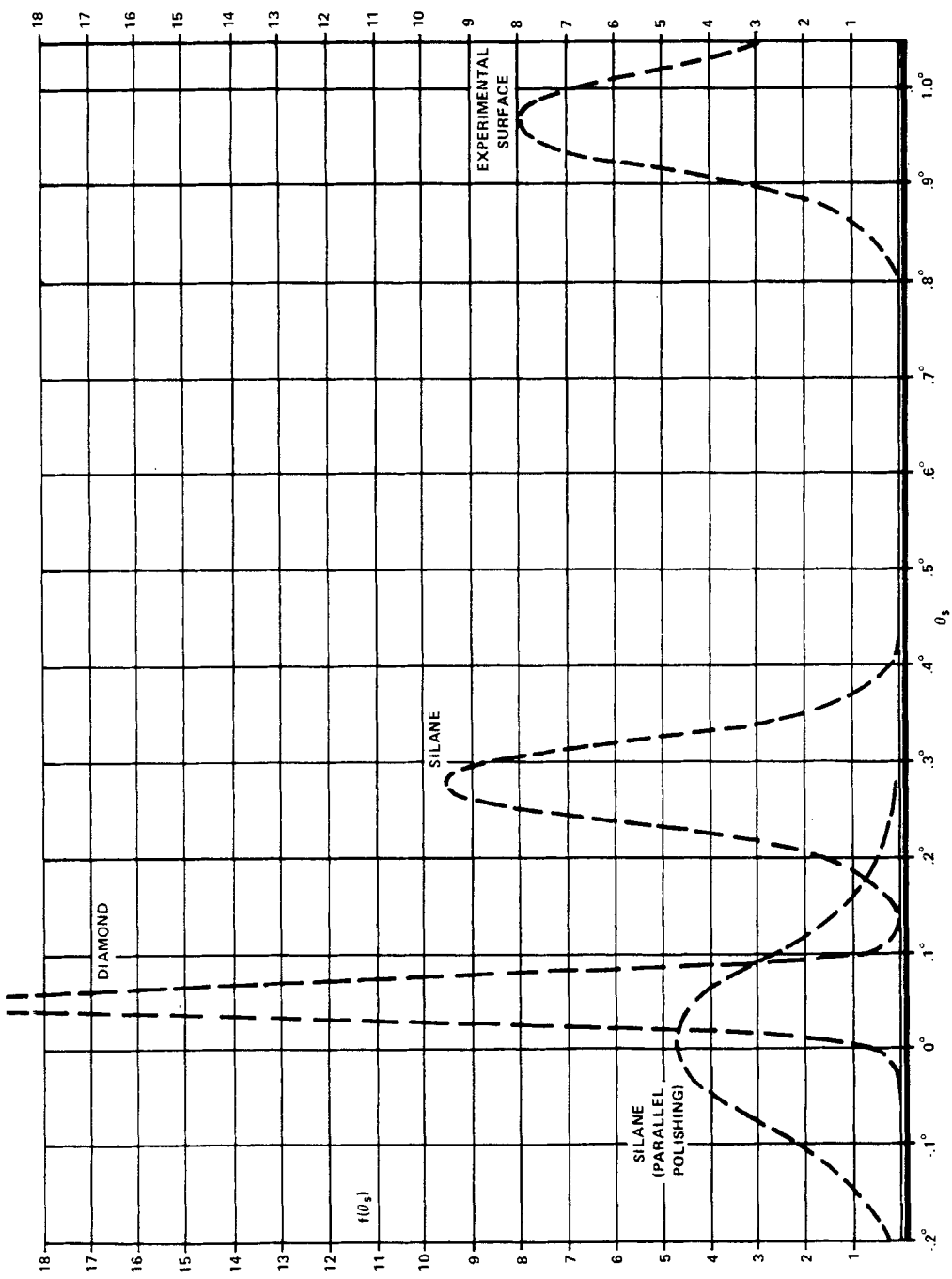

Two silane surfactant treated surfaces are shown. Cell construction was identical to that of the "Diamond" samples, including the diamond polish, but were subsequently treated with the silane surfactant. The silane used, referred to as. 2024 silane, was N-methl-3-aminopropyltrimethoxysilane. After the diamond polishing, the cells were soaked in a 0.25% aqueous solution of the silane and then were dry polished on a lint free cloth such as "Opticloth." A 150°C bake in N_2 completed the processing before assembly.

A substantial improvement in tilt preference results from the silane treatment. Also shown is a cell processed an identical manner except that opposing polishing directions in the sense of Figure 4 were used; this results in virtually no tilt preference and a broader variance.

The final curve, marked experimental surface, demonstrates an even larger tilt preference. Instead of a SiO_2 coating over the electrodes, a polyamide-imide copolymer coating, Rhodia Kermid #500, was used. The coating was spun on and then cured at 250°C for about one hour. Polishing was performed with lens paper and then assembled.

APPLICATION TO SURFACE STUDIES

The previous experimental results point out promising utilizations of this technique to evaluate surfaces. All of the results described above utilized the *same* liquid crystal but the surfaces were varied. It should be pointed out that the representative surfaces described above are truly representative; a given technique repeated over and over again consistently falls very close to these curves therefore the differences are truly describing different surface conditions.

Other possibilities are to use a standard technique and vary the liquid crystal. Also, aging and degradation may be evaluated by repeating the measurements on stressed cells.

Bibliography

1. R. W. Gurtler and C. Maze, *IEEE Spectrum*, **25**, Nov. 1972.
2. F. C. Frank, *Discussions Faraday Soc.*, **25**, 19, 1958.
3. W. Helfrich, *Mol. Crys. Liquid Cryst.*, **21**, 187, 1973.